Crystal Structure of the *S*-Adenosylmethionine Synthetase Ternary Complex: A Novel Catalytic Mechanism of *S*-Adenosylmethionine Synthesis from ATP and Met[†,‡]

Junichi Komoto,[#] Taro Yamada,[#] Yoshimi Takata,[#] George D. Markham,[§] and Fusao Takusagawa*[,#]

Department of Molecular Biosciences, University of Kansas, 1200 Sunnyside Avenue, Lawrence, Kansas 66045-7534, USA, and The Institute for Cancer Research, The Fox Chase Cancer Center, Philadelphia, Pennsylvania 19111, USA

Received September 7, 2003; Revised Manuscript Received December 11, 2003

ABSTRACT: *S*-Adenosylmethionine synthetase (MAT) catalyzes formation of *S*-adenosylmethionine (SAM) from ATP and L-methionine (Met) and hydrolysis of tripolyphosphate to PP_i and P_i. *Escherichia coli* MAT (eMAT) has been crystallized with the ATP analogue AMPPNP and Met, and the crystal structure has been determined at 2.5 Å resolution. eMAT is a dimer of dimers and has a 222 symmetry. Each active site contains the products SAM and PPNP. A modeling study indicates that the substrates (AMPPNP and Met) can bind at the same sites as the products, and only a small conformation change of the ribose ring is needed for conversion of the substrates to the products. On the basis of the ternary complex structure and a modeling study, a novel catalytic mechanism of SAM formation is proposed. In the mechanism, neutral His14 acts as an acid to cleave the C5′−O5′ bond of ATP while simultaneously a change in the ribose ring conformation from C4′-*exo* to C3′-*endo* occurs, and the S of Met makes a nucleophilic attack on the C5′ to form SAM. All essential amino acid residues for substrate binding found in eMAT are conserved in the rat liver enzyme, indicating that the bacterial and mammalian enzymes have the same catalytic mechanism. However, a catalytic mechanism proposed recently by González et al. based on the structures of three ternary complexes of rat liver MAT [González, B., Pajares, M. A., Hermoso, J. A., Guillerm, D., Guillerm, G., and Sanz-Aparicio. J. (2003) *J. Mol. Biol. 331*, 407] is substantially different from our mechanism.

In biological systems, there are a myriad of reactions in which methyl groups are transferred from a few types of methyl donors to a wide variety of methyl acceptors. Among biological methyl group donors, *S*-adenosylmethionine (SAM),[1] discovered by Cantoni in 1953 (*1*), is the most widely used, while 5-methyltetrahydrofolic acid, methylcobalamin, and betaine are involved in far fewer methylation reactions.

The formation of SAM is catalyzed solely by *S*-adenosylmethionine synthetase (MAT, ATP:L-methionine *S*-adenosyltransferase, EC 2.5.1.6), and occurs in an unusual two-step reaction in which the complete tripolyphosphate chain is cleaved from ATP as SAM is formed, and the tripolyphosphate is further hydrolyzed to PP_i and P_i before the sulfonium product (SAM) is released, giving the overall reaction shown (*2*).

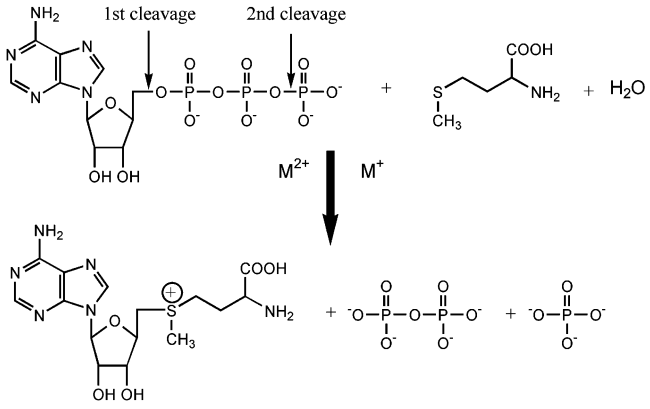

Thus, the enzyme must catalyze reactions at both ends of the tripolyphosphate chain, which appears to be a unique catalytic task. The SAM forming reaction was found by stereochemical and kinetic isotope studies to occur as an S_N2 reaction with direct attack of the sulfur of methionine on

[†] The work has been supported by NIH Grants GM37233 (F.T.) and GM31186 (G.D.M.).

[‡] The atomic coordinates and structure factors have been deposited with the Protein Data Bank (entry name: 1P7L and 1RG9).

* To whom all correspondence should be addressed. Department of Molecular Biosciences, University of Kansas, 1200 Sunnyside Ave., Lawrence, KS 66045-7534, USA; tel: (785) 864-4727; e-mail: xraymain@ku.edu.

[#] University of Kansas.

[§] The Fox Chase Cancer Center.

[1] Abbreviations: MAT, *S*-adenosylmethionine synthetase; eMAT, MAT from *E. coli*; rMAT, MAT from rat liver; SAM, *S*-adenosylmethionine; SAH, *S*-adenosylhomocysteine; Met, L-methionine; AMB, L-2-amino-4-methoxy-*cis*-but-3-enoic acid; AEP, (2*S*,4*S*)-amino-4,5-epoxypentanoic acid; P_i, orthophosphate; PP_i, pyrophosphate; PPP_i, tripolyphosphate; PPNP, imido-triphosphate; AMPPNP, 5′-adenyl imido-triphosphate; eMAT:($2P_i$), eMAT complexed with two P_i; eMAT:(PP_i+P_i), eMAT complexed with PP_i and P_i; eMAT:(ADP+P_i), eMAT complexed with ADP and P_i; eMAT:(AMPPNP+Met), eMAT complexed with AMPPNP and Met; eMAT:(SAM+PPNP), eMAT complexed with SAM and PPNP; rMAT:(AMB+$2SO_4$), rMAT complexed with AMB and two SO_4^{2-} ions; rMAT:(AEP+$3PO_4$), rMAT complexed with AEP and three P_i; rMAT:(ATP+Met+$2P_i$), rMAT complexed with ATP, Met, and $2P_i$; rMAT:(ATP+AEP+$2P_i$), rMAT complexed with ATP, AEP, and $2P_i$; rMAT:(ADP+AMB+$3P_i$), rMAT complexed with ADP, AMB, and $3P_i$; flexible loop, loop composed of amino acid residues 98−108.

10.1021/bi035611t CCC: $27.50
Published on Web 01/27/2004

the C5′ atom of ATP (*3*, *4*). Cantoni originally reported that divalent metals are essential for activity (*1*). Details of the catalytic mechanism of MAT have been studied by using various methods including kinetic measurements (*5*, *6*), EPR spectroscopic studies (*7*, *8*), mutagenesis studies (*9*−*13*), computational modeling studies (*14*), NMR studies (*15*), and numerous inhibition studies by Met and ATP analogues that have inhibitory activity against the enzyme (*16*−*20*).

The first crystal structure of eMAT containing two P_i showed a unique polypeptide folding including a knot formation at the N-terminus (*21*, *22*). The second crystal structure of eMAT crystallized with ATP contained ADP and P_i in the active site (eMAT:(ADP+P_i)), and showed a possible PPP_i binding site of ATP, but the binding site of the adenosine moiety was not clearly identified due to disorder (*23*). A loop (flexible loop) composed of the amino acid residues 98−108 was disordered in the eMAT structures. The substrate-free eMAT structure showed that the flexible loop hung above the active site, and was involved in the catalytic activity (*24*). Recently, the crystal structure of rat liver MAT complexed with a methionine analogue L-2-amino-4-methoxy-*cis*-but-3-enoic acid (AMB), rMAT:(AMB+2SO_4), has been determined at 2.7 Å resolution (*25*). rMAT has 15 additional amino acid residues at the N-terminus with respect to eMAT, and the polypeptide folds in the same fashion as observed in eMAT. Therefore, the structure of rMAT confirms the unusual knot structure found in the N-terminal section of eMAT structure. From the rMAT:(AMB+2SO_4) structure, the Met binding site and the disulfide linkage that differentiates rMAT I (a tetramer) and rMAT III (a dimer composed of the same subunit) have been proposed.

When AMPPNP instead of ATP is used along with Met as the substrates, SAM formation occurs but the PPNP hydrolysis is inhibited (*5*). Thus, crystals of a stable ternary complex can be grown from the solution containing eMAT, AMPPNP, and Met. Here we report a crystal structure of eMAT ternary complex (eMAT:(SAM+PPNP)). On the basis of the new structure, a detailed catalytic mechanism of SAM formation is proposed.

It is noted that three ternary complex structures of rMAT have recently been published (*26*). The locations of ATP and Met binding sites are completely different from the sites seen in the *Escherichia coli* enzyme. The structures of the rMAT complexes have several unusual features, such as unreacted ATP and Met in the active site and very large temperature factors of the molecules and ions in the active site. The proposed catalytic mechanism based on those ternary complex structures is substantially different from our mechanism and requires a large movement of ATP within the active site (*26*).

EXPERIMENTAL PROCEDURES

Crystallization. eMAT was prepared from *E. coli* strain DM50pK8, a strain that harbors the plasmid pK8 which contains the structural gene for the enzyme. The enzyme was purified to electrophoretic homogeneity using methods previously described (*5*). A mixture of eMAT (36 mg/mL), AMPPNP (5 mM), and Met (10 mM) in 50 mM Hepes-K^+ buffer pH 8.0 containing KCl (50 mM), $MgCl_2$ (10 mM), and DTT (5 mM) was incubated for 60 min at 37 °C. The mixture was diluted with 50 mM Hepes-K^+ buffer to a protein concentration of 20 mg/mL. Hanging drops were made with equal volumes of the protein mixture and a crystallization solution containing 8%(v/w) PEG-8000, 50 mM Tris/HCl pH 8.0, 200 mM KCl, 1 mM DTT, and 20% ethylene glycol. Thick plate shaped crystals suitable for X-ray diffraction studies were grown at 23 °C for 1 day.

Table 1: Crystallographic Statistics[a]

resolution (Å)	50−2.5
total observations	165,302
unique reflections	46,081
completeness (%)	95.0
R_{sym} (%)[b]/outer shell[d]	9.3/18.7
no. subunits in asymmetric unit	4
protein non-hydrogen atoms	11768
substrates (AMPPNP and Met)	2 and 2
products (SAM and PPNP)	2 and 2
K^+ ions and Mg^{2+} ions	4 and 8
solvent molecules (H_2O)	20
resolution range (Å)	10.0−2.5
total reflections used in R_{cryst}	40,557
total reflections used in R_{free}	4,056
R_{cryst}[c] (outer shell)[d]	0.213 (0.285)
R_{free} (outer shell)[d]	0.242 (0.365)
Rmsd of bond distances (Å)	0.009
Rmsd of bond angles (°)	1.36
Rmsd of torsion angles (°)	27.5
most favored region (%) of Ramachandran plot	89.7
additional allowed region (%) of Ramachandran plot	10.3

[a] Space group: $P2_12_12_1$; unit cell dimension: $a = 225.82$, $b = 69.13$, $c = 118.23$ Å; M_r of subunit: 42130; no. subunits in the unit cell: 16; $V_M = 2.74$ Å^3; percentage of solvent content: 55%. [b] $R_{sym} = \sum_h\sum_i|I_{hi} - \langle I_h\rangle|/\sum_h\sum_i|I_{hi}|$. [c] $R_{cryst} = \Sigma||F_o| - |F_c||/\Sigma|F_o|$. [d] Outer shell = 2.5−2.61 Å resolution.

Data Measurement. A crystal (∼0.3 × 0.3 × 0.1 mm) in a hanging drop was scooped up with a nylon loop and was frozen in cold nitrogen gas (−180 °C) on a Rigaku RAXIS imaging plate X-ray diffractometer with a rotating anode X-ray generator as an X-ray source (CuK_α radiation operated at 50 KV and 100 mA). The X-ray beam was focused to 0.3 mm by confocal optics (Osmic, Inc., USA). The diffraction data were measured up to 2.5 Å resolution at −180 °C. The data were processed with the program DENZO/SCALEPACK (*27*). Data statistics are given in Table 1. It is noted that the unit cell dimensions were determined during examination of crystal qualities, and most of those values were significantly different from each other, indicating that the eMAT complexes can pack differently in the crystals.

Crystal Structure Determination. The unit cell dimensions and space group ($P2_12_12_1$) indicate that an asymmetric unit contains one tetrameric enzyme. The crystal structure was determined by a molecular replacement procedure using an eMAT dimer as the search model. The model structure was refined with the POSITIONAL protocol and then the simulated annealing procedure of X-PLOR (*28*). The missing polypeptide chain for the amino acid residues 98−108 was built in ($2F_o - F_c$) maps. ($2F_o - F_c$) and ($F_o - F_c$) maps showed two large significant residual electron density peaks in the region of active site (Figure 1). Since eMAT was crystallized in the presence of an excess of AMPPNP (5 mM) and L-Met (10 mM) and a characterization study has suggested that the substrates are rapidly converted to the products (SAM and PPNP) in the active site (*5*), these peaks were assigned to SAM and PPNP. The model containing

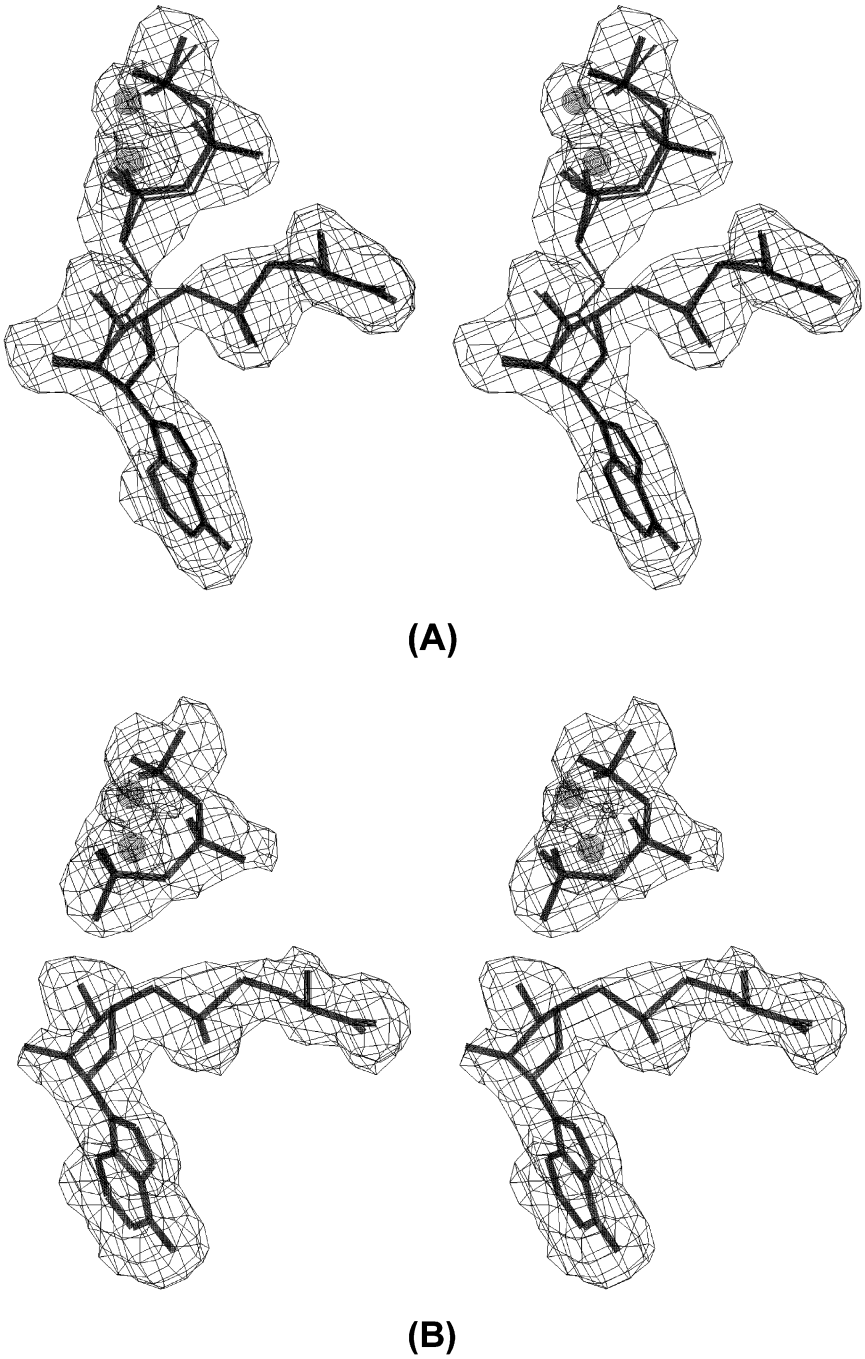

FIGURE 1: ($F_o - F_c$) maps showing residual electron density peaks in dimer AB (A) and in dimer CD (B). The final SAM and PPN models (thick lines) are superimposed in the residual density peaks, while AMPPNP and Met models (thin lines) are superimposed in the residual electron density peaks in dimer AB. Two Mg ions bound to PPNP are indicated by ●. The contours are drawn at 2.5 σ level.

the products in the active sites was refined with the simulated annealing procedures of X-PLOR. During the refinement, the model structure was restrained by 222 noncrystallographic symmetries. Two residual peaks near the PPNP moiety in each subunit were assigned to Mg^{2+} ions. The highest residual peak except for the products in the each active site was assigned to the K^+ ion. The Mg^{2+} and K^+ ions were located at the same sites in all four subunits. Other well-defined residual peaks in the active sites were assigned to water molecules. Each monomer including products and metal ions in the dimer were restrained by a noncrystallographic symmetry (NCS). The NCS weight in the X-PLOR refinement was set to 100. The model was refined with all data (no sigma cut) within a 2.5 Å resolution.

A Modeling of eMAT:(AMPPNP+Met). As shown in Figure 1, the residual electron density peaks in the dimer AB suggested a possibility of the substrates (AMPPNP and Met) in the active site. Therefore, the model containing the substrates in the dimer AB and the products in the dimer CD was refined by the same procedures described above. Compared to the eMAT:(SAM+PPNP) structure, there was no significant movement of atoms except for C5′ of the adenosine moiety of AMPPNP. The R and R_{free} values did not changed. A superimposed view of the products and substrates is shown in Figures 1 and 2. The refined coordinates are deposited along with the coordinates containing the products (SAM and PPNP) in the both dimers (PDB code: 1P7L, 1RG9).

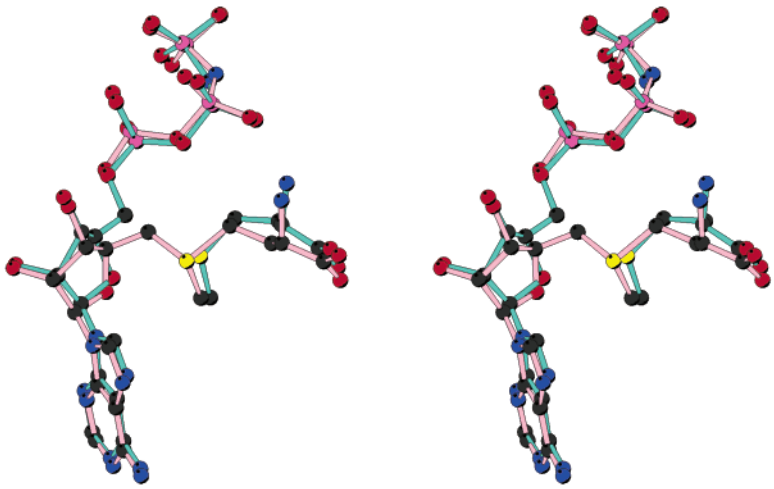

FIGURE 2: A superimposed view of the substrates (AMPPNP and Met) obtained by a modeling and the products (SAM and PPNP) showing that the substrates can convert to the products without any major changes in the active site. The substrates and products are drawn with aquamarine and light-pink bonds, respectively.

RESULTS

Overall Structure. The crystallographic refinement parameters (Table 1), final ($2F_o - F_c$) maps, and conformational analysis by PROCHECK (*29*) indicate that the crystal structure of a ternary complex eMAT:(SAM+PPNP) has been determined successfully. The crystal structure contains one tetramer (i.e., four identical subunits) in the asymmetric unit. The two subunits A and B interact with each other relatively strongly and form a dimer. Similarly, C and D form a dimer as well. The contact surfaces between the two subunits A and B, and the two dimers AB and CD are calculated to be 2700 and 1800 Å^2, respectively (*30*). Thus, eMAT is a dimer of dimers and has a noncrystallographic 222 symmetry. The four subunits are structurally identical with the maximum rmsd of 0.13 Å. The rmsd between two dimers (AB and CD) is 0.18 Å, indicating that the two dimers have the same subunit associations. The polypeptide-folding scheme of each subunit is similar to those of complexes of eMAT:(2P$_i$) (*21*), eMAT:(ADP+P$_i$) (*23*), rMAT:(AMB+2SO$_4$) (*25*), rMAT:(AEP+3PO$_4$) (*26*), rMAT:(ATP+Met) (*26*), rMAT:(ATP+AEP) (*26*), and rMAT:(ADP+AMB) (*26*). Two active sites are located between two subunits forming a dimer. Each active site contains the products SAM and PPNP. The electron density peaks of SAM and PPNP in dimer AB and in dimer CD are shown in Figure 1. Since the active sites are formed with amino acid residues from the two subunits, the amino acid residue number with an asterisk indicates that it belongs to the partner subunit of the dimer.

Active Site Contents. SAM formation from ATP and Met catalyzed by MAT is a two-step reaction as illustrated in the introduction. The overall reaction is an exergonic process because of the PPP$_i$ hydrolysis. Since eMAT cannot hydrolyze the γ-phosphate of the PPNP group cleaved from AMPPNP, the catalytic reaction stops after formation of SAM and PPNP (*5*). The products are trapped in the active site because the PPP$_i$ hydrolysis energy is not available. For this reason, the active sites of eMAT should contain SAM and PPNP. Indeed, the ($F_o - F_c$) maps show clearly the products (SAM and PPNP) in the active sites of dimer CD (Figure 1). However, the residual electron density peaks in dimer AB show two possibilities (i.e., substrate (AMPPNP and Met) or products (SAM and PPNP)). In the crystal structure, dimer AB has more contacts with neighboring molecules than dimer CD does, suggesting that dimer CD has more vibrational freedom than dimer AB in the crystal. Indeed, the mean temperature factor of dimer CD is significantly larger than that of dimer AB (23.6 vs 15.5 Å^2). When molecular packing forces reduce the thermal vibration of the enzyme, the reverse reaction could occur and the trapped products (SAM and PPNP) could move back to the substrate (AMPPNP and Met) in the active site.

On the basis of the above assumption, the model containing the substrates in dimer AB and the products in dimer CD was refined by the same procedures in the experimental section. Compared to the eMAT:(SAM+PPNP) structure, there was no significant movement of atoms except for the C5′ of the adenosine moiety of AMPPNP (Figure 2). The substrates (AMPPNP and Met) maintain the exact same hydrogen bonds with the enzyme as observed in the product structure. The R and R_{free} values did not change, indicating that it is impossible to determine the actual contents in the active site by the X-ray analysis. However, this modeling attempt indicates that the substrates (AMPPNP and Met) can bind at the same sites as the products and only a small conformation change of the ribose ring is needed in conversion of the substrates to the products. The ribose ring of SAM has a C3′-*endo* conformation (^{3}E, $P = 18°$, $\tau = 40°$) and the C5′ is connected to the S$_D$ of Met, whereas the ribose ring in AMPPNP has a C4′-*exo* conformation ($_4$E, phase angle of pseudorotation ($P = 53°$, puckering amplitude $\tau = 56°$) and the C5′ is connected to the O5′ of PPNP. This difference in the ribose ring conformations of bound AMPPNP and SAM is consistent with that seen in previous NMR studies (*15*).

Interactions between the Enzyme and Products in the Active Site. Figure 3 shows the possible hydrogen bonds between the products and eMAT. The adenine ring of SAM is recognized by a hydrogen bond (N6···O[Arg229]) and a stacking interaction with the phenyl ring of Phe230. There are three water binding sites (Wat411, Wat413, and Wat416) around the adenine ring. The Wat$_{411}$ site near the N1 is

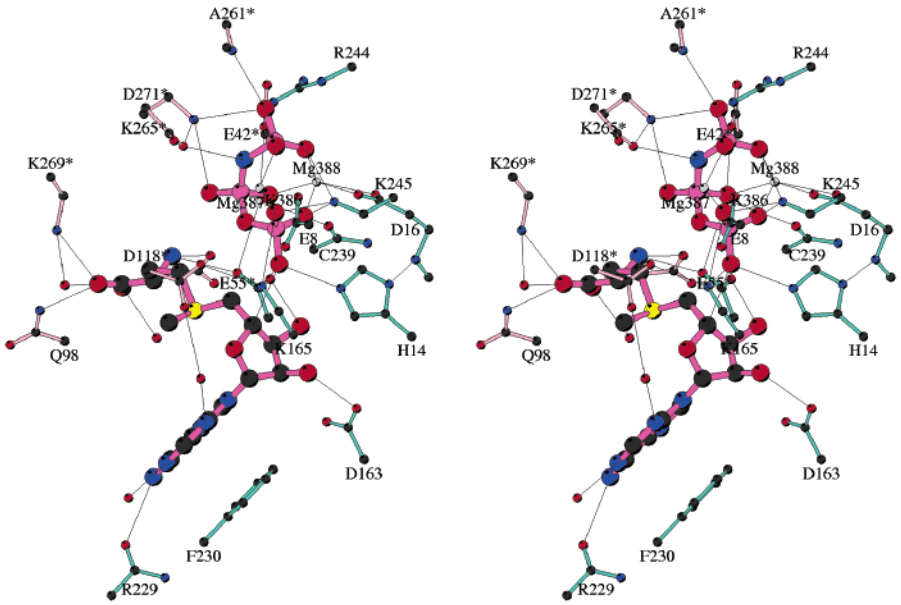

(A)

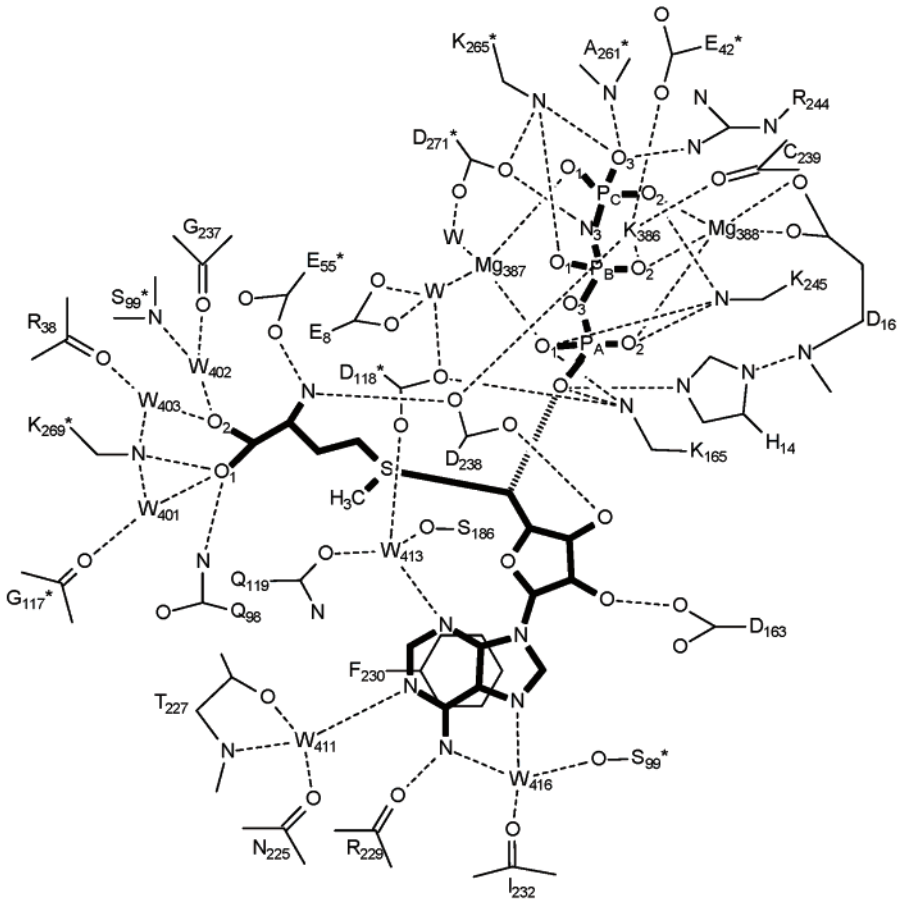

(B)

FIGURE 3: Active site geometry. Thin lines illustrate possible hydrogen bonds and ionic bonds between the products and protein. (A) Amino acid residues that belong to subunits A/C and B/D are drawn with green and light-pink bonds, respectively. The bonds in the products (SAM and PPNP) are magenta. The amino acid residues with an asterisk belong to subunit B/D. (B) Schematic illustration showing possible hydrogen bonds and ionic bonds between the substrates/products and the amino acid residues composing the active site. W_{401}−W_{416} are the water binding sites, and K_{386} is a potassium ion. The distances of C5′−S_D and C5′···O_{4A} in the products (SAM and PPNP) are 1.74 and 2.93 Å, respectively. The same hydrogen bonds and ionic bonds are observed in a model structure of eMAT:(AMPPNP+Met), and the distances of C5′−O5′ and C5′···S_D are 1.51 and 3.12 Å, respectively.

surrounded by O[Asn225], N[Thr227], and O_G[Thr227]. The Wat_{411} sites in all subunits are occupied by a water molecule. The Wat413 site near N3 is surrounded by O_{D1}[Asp118*], OE1[Gln119*], and O_G[Ser186]. The Wat413 sites in subunits A and B are occupied by a water molecule. The Wat416 site near N6 and N7 is surrounded by O_G[Ser99*] and O[Ile232]. The Wat416 sites in subunits C and D are also occupied by a water molecule. These water-mediated hydrogen bonds connect the adenine ring to the protein. The 2′-OH and 3′-OH of adenosine ribose interact with the two acidic amino acid residues Asp163 and Asp238 (O2′···O_{D1}-[Asp163] and O3′···O_{D2}[Asp238]). Similar interactions between the OH groups of SAM/SAH and the acidic amino acid residues are seen in the structures of methyltransferase: SAM/SAH complexes (*31*−*48*).

The Met moiety is recognized by four hydrogen bonds, in which the amino group (N) forms hydrogen bonds with the acidic amino acid residues (N···O_{E2}[Glu55*] and N···O_{D1}[Asp238]), and the carboxylate group forms hydrogen bonds with the neutral/basic amino acid residues (O_1···N_{E2}[Gln98*] and O_1···N_Z[Lys269*]). In addition to these hydrogen bonds, two water molecules form hydrogen bonds with O_1 and O_2, respectively. One water molecule is located in the Wat401 site in the all subunits and is connected to O[Gly117*] and N_Z[Lys269*]. The other water molecule occupies the Wat402 site in subunits A and B or the Wat403 site in subunits C and D. The Wat402 and Wat403 sites are surrounded by N[Ser99*] and O[Gly237], and by O[Arg38] and N_Z[Lys269*], respectively. Apparently, the Met moiety of SAM is tightly bound to the protein by direct and water-mediated hydrogen bonds.

As shown in Figure 3, the PPNP ion is heavily involved in hydrogen bonds and ionic bonds. The PPNP ion has a U-shaped conformation. Two magnesium ions (Mg^{2+}) interact with the phosphate oxygens from both sides of the U-shaped PPNP ion. One of the magnesium ions (Mg387) makes two ionic bonds with O_{1A} and O_{1C}, and is surrounded by Glu8, Asp118*, and Asp271*. The carboxylate groups of Glu8, Asp118*, and Asp271* are located outside the ionic bond distance to Mg387, indicating that a few disordered water molecules are located between the carboxylate groups and the Mg^{2+} ion. The other magnesium ion (Mg388) is held by Asp16 and forms three ionic bonds with three oxygens (O_{2A}, O_{2B}, and O_{2C}). It is noted that the coordination geometries of these Mg^{2+} ions are not an idealized bipyramid due to disordered water molecules surrounding the Mg^{2+} ions. One potassium ion (K^+) is located near O_{2B} and is surrounded by three additional oxygens (O_{E2}[Glu42*], O_{D1}[Asp238], and O[Cys239]). The K···O interactions are apparently weak (K···O distances are 2.8 ∼ 3.5 Å), and the K^+ ion is far from the catalytic site, suggesting that it is not directly involved in the catalytic reaction. Indeed, a relatively high concentration of K^+ (> 5 mM) is required for the half-maximal activation (*5*). Therefore, the role of the K^+ ion in the active site appears to be the maintenance of the active site geometry rather than the stabilization of the negatively charged PPP_i moiety for the catalysis.

The P_A phosphate moiety interacts with three basic amino acid residues with five hydrogen bonds (O_{4A}···N_{E2}[His14], O_{1A}···N_Z[Lys165], O_{4A}···N_Z[Lys165], O_{1A}···N_Z[Lys245], O_{2A}···N_Z[Lys245]). Similarly, the P_C phosphate moiety interacts with three basic amino acid residues/group through four hydrogen bonds (O_{3C}···N_{H2}[Arg244], O_{2C}···N_Z[Lys245], O_{3C}···N_Z[Lys265*], and O_{3C}···N[Ala261*]). The bridging nitrogen N_{3B} makes a hydrogen bond with an acidic amino acid residue Asp271* (N_{3B}···O_{D1}[Asp271*]). The C4′-H of ribose points to O_{4A} of the P_A phosphate with the C4′···O_{4A} distance of 3.1 Å, suggesting a C−H···O hydrogen bond. It is noted that, without any exception, the basic and acidic groups of the Met and PPNP moieties interact with acidic and basic amino acid residues, respectively, suggesting that the structure of a ternary complex of eMAT has been determined successfully. All essential amino acid residues for substrate binding found in the *E. coli* enzyme are conserved in the rat liver enzyme, indicating that the bacterial and mammalian enzymes have a similar catalytic mechanism (Table 2).

Table 2: Sequence Agreement between eMAT and rMAT at the Essential Amino Acid Residues for Substrate Binding[a]

residue site	H-bond or ionic bond partner	*E. coli* MAT	rat liver MAT
His14	O_{4A}	^{12}**EGHPK**^{17}	^{28}**EGHPK**^{32}
Asp16	Mg^{2+} (Mg388)	^{14}**HPDKI**^{18}	^{30}**HPDKI**^{34}
Glu_{42}	K^+ (K386)	^{40}**ACET**y^{44}	^{56}**ACET**v^{60}
Glu_{55}	N	^{53}g**GEIT**^{57}	^{69}c**GEIT**^{73}
Gln98	O_1	^{96}**In**Q**g**V^{100}	^{118}**Ia**Q**c**V^{122}
Asp163	$O_{2'}$	^{161}**RPDaK**^{165}	^{178}**RPDsK**^{182}
Lys165	O_{1A}, O_{4A}(O5′)	^{163}**DaKsQ**^{167}	^{180}**DsKtQ**^{184}
Phe230	stacked with adenine ring	^{228}**GRFVI**^{232}	^{249}**GRFVI**^{253}
Asp238	$O_{3'}$, K^+ (K386)	^{236}m**GDc**G^{240}	^{257}q**GDa**G^{261}
Arg244	O_{3C}	^{242}**TGRKI**^{246}	^{263}**TGRKI**^{267}
Lys245	O_{1A}, O_{2A}	^{243}**GRKII**^{247}	^{264}**GRKII**^{268}
Lys_{265}	O_{1B}, O_{3C}	^{263}**SGKD**p^{267}	^{284}**SGKD**y^{288}
Lys_{269}	O_1	^{267}ps**KVD**^{271}	^{288}yt**KVD**^{292}
Asp_{271}	N_{3B}	^{269}**KVDRS**^{273}	^{290}**KVDRS**^{294}

[a] The conserved amino acid residues are represented by bold capital letters, and the start and ending sequence numbers are shown on the left and right sides, respectively.

A Role of the Flexible Loop (Residues 98−*108).* As shown in Figure 4, the products are completely surrounded by amino acid residues, and thus the apparent entrance of the active site is not recognizable in the ternary complex structure. On the other hand, the flexible loop composed of the amino acid residues 98−108 is disordered in the binary complex structures, and thus the entrance to the active site is clearly recognizable. Therefore, the flexible loop acts as a gate to the active site. Since the flexible section does not have any contacts with the neighboring molecules in the crystal structure, the order−disorder conformational change of the flexible loop is not due to the crystal packing effects.

DISCUSSION

Differences between the eMAT Ternary and Binary Complex Structures. The crystal structures of eMAT binary complexes, eMAT:($2P_i$), eMAT:(PP_i+P_i), eMAT:(ADP+P_i), have been determined (*21*, *23*). Since these structures are very similar to each other including the P_i and PP_i binding sites, we will compare the structure of eMAT:(ADP+P_i) to the structure of eMAT:(SAM+PPNP). The overall polypeptide folding of eMAT in the complexes is quite similar, except for the flexible loop composed of the amino acid residues 98−108. The flexible loop is ordered in eMAT:(SAM+PPNP), whereas the same loop is invisible (disordered) in the other eMAT and rMAT structures. The ordered

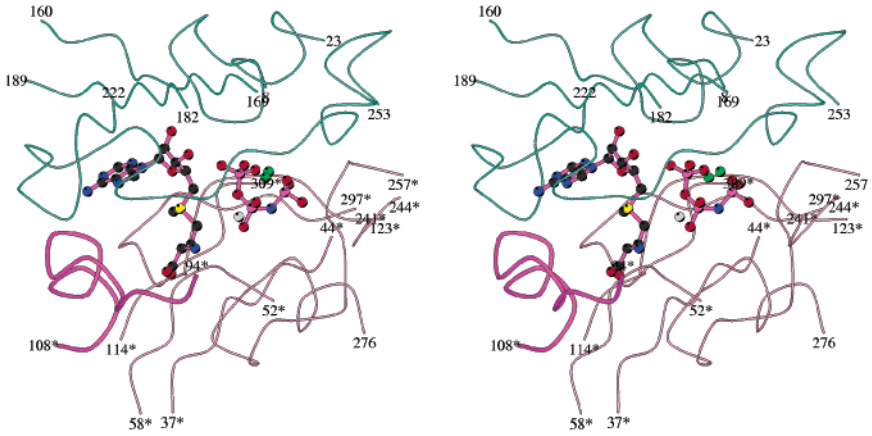

FIGURE 4: SAM and PPNP in the active site showing no apparent entrance of the active site. The flexible loop which acts as a gate to the active site is shown by a thick coil (magenta color). Subunits A and B are illustrated by green and light-pink coils.

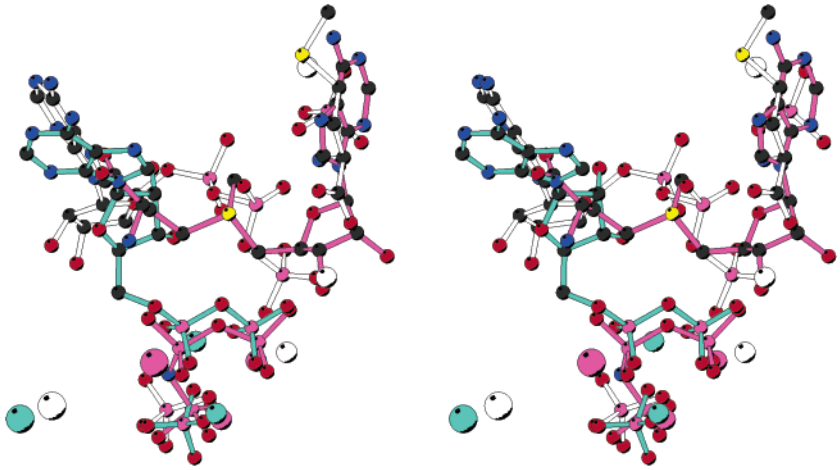

FIGURE 5: A superimposed active site view of the molecules and ions in the active sites of eMAT:(SAM+PPNP), eMAT:(ADP+P_i), and rMAT:(ATP+Met+2P_i) showing the relative locations of SAM, PPNP, ADP, ATP, Met, P_i, Mg^{2+} ions, and K^+ ions in the active site. The active site contents of eMAT:(SAM+PPNP), eMAT:(ADP+P_i), and rMAT:(ATP+Met+2P_i) are illustrated by magenta, aquamarine, and white colored bonds, respectively. The Mg^{2+} and K^+ ions are illustrated by small and large circles, respectively. The C_A atoms of eMAT:(ADP+P_i) and rMAT:(ATP+Met) were superimposed on the corresponding C_A atoms of eMAT:(SAM+PPNP) by a least-squares method, and the protein parts were removed from the figure.

flexible loop in eMAT:(SAM+PPNP) partially occupies the adenine ring binding site seen in eMAT:(ADP+P_i). A superimposed view of the active sites of eMAT:(SAM+PPNP) and eMAT:(ADP+P_i) is shown in Figure 5.

The PPNP ion binds at the same site of diphosphate of ADP seen in eMAT(ADP+P_i). However, the orientation of the pyrophosphate moiety of ADP is reversed (i.e., the α- and *β*-phosphates of ADP superimpose on the *β*- and α-phosphate sites of PPNP, respectively). For this reason, the adenosine moiety of ADP lies on the opposite side of the active site. The bound Met occupies the adenosine binding site seen in eMAT:(ADP+P_i). Mg^{2+} ions in both eMAT:(ADP+P_i) and eMAT:(SAM+PPNP) bind around the P_i, PP_i, and PPNP moieties. There are significant differences in the K^+ binding sites in the binary and ternary complexes.

As seen in Figure 5 and described above, there are several significant differences among the active site structures of eMAT:(SAM+PPNP) and eMAT:(ADP+P_i). One difference is the adenosine moiety binding sites in the structures of eMAT:(SAM+PPNP) and eMAT:(ADP+P_i). This could be due to the differences between the binary and ternary complexes. There is a relatively large empty space in the active site of the binary eMAT:(ADP+P_i) complex, and thus, the adenosine moiety of ADP can be located in several sites (i.e., disorder), which is consistent with the known very low affinity of the enzyme for ADP (a K_i > 10 mM compared to the ATP K_M of 0.1 mM) (*5*). On the other hand, there is no empty space in the ternary eMAT:(SAM+PPNP) complex, and thus the adenosine moiety of SAM and the Met must locate their correct sites to fit into the active site. Indeed, the adenosine moiety of ADP has relatively large temperature factors (the mean temperature factor is above 100 Å^2, although that of pyrophosphate moiety is 30 Å^2) and has little interaction with the protein, indicating that the adenosine moiety is disordered. In eMAT:(SAM+PPNP), the adenosine moiety of SAM has a well-defined electron density and is ordered (the mean temperature factor is 13.5 Å^2).

From a functional standpoint, another explanation is that the MAT active site is designed to differentiate between ADP and ATP since ATP and AMPPNP are substrates but ADP is neither a substrate nor an inhibitor. As will be described below, if ADP bound to MAT in the same way as AMPPNP, ADP would be a substrate.

Differences between the eMAT and rMAT Ternary Complex Structures. Recently, González et al. published two binary and three ternary complex structures of rMAT (*25*,

Table 3: A Comparison of eMAT and rMAT Ternary Complexes

complex	PDB code	resolution (Å)	mean *B* value of protein (Å^2)	mean *B* value of the molecules and ions in the active site (Å^2)	C5′···S_D/O_D or C5′···O5′ distance (Å)
eMAT:(SAM+PPNP)	1P7L	2.50	19.6	13.3	2.93
rMAT:(ATP+Met+2P_i)	1O9T	2.90	37.0	82.4	9.60
rMAT:(ATP+AEP+2P_i)	1O93	3.49	27.8	20[a]	8.82
rMAT:(ADP+AMB+3P_i)	1O92	3.19	24.6	74.3	9.84
rMAT:(AMB+2SO_4)	1QM4	2.66	31.4	46.6	*b*
rMAT:(AEP+3PO_4)	1O90	3.10	33.6	78.1	*b*

[a] The temperature factors of the molecules and ions in the active site are assigned to 20 Å^2 and are apparently not the refined values. [b] A binary complex.

26), each with additional active site bound anions. Those are rMAT:(AMB+2SO_4), rMAT:(AEP+3PO_4), rMAT:(ATP+Met+2P_i), rMAT:(ATP+AEP+2P_i), and rMAT:(ADP+AMB+3P_i). The crystals of these complexes were isomorphous to each other, but not to the eMAT complexes. The rMAT is also a tetramer and has a 222 symmetry. The crystallographic asymmetric unit contains one dimer, and two dimers are related by the crystallographic 2-fold axis. The N-terminal residues and the flexible loop are disordered. Although polypeptide folding in rMAT is very similar to that of eMAT, the binding sites of molecules and ions in the active sites of the rMAT ternary complexes are quite different from the corresponding sites seen in eMAT:(SAM+PPNP) (Figure 5). There are five unusual features in the rMAT ternary complexes (rMAT:(ATP+Met+2P_i), rMAT:(ATP+AEP+2P_i), rMAT:(ADP+AMB+3P_i)) (*26*). Those are the following:

(i) Although MAT has a 222 symmetry and obeys hyperbolic kinetics, one of the two active sites of the dimer is always empty.

(ii) Although the catalytic rate of MAT is faster than one turnover per second, one complex contains the substrates (ATP and Met) in the active site.

(iii) Although P_i is a competitive inhibitor of ATP, the ternary complexes contain both ATP and P_i in the active site.

(iv) Many charged groups in the active site do not interact with charged amino acid residues.

(v) The average temperature factor of the molecules and ions in the active is much higher than that of the protein (see Table 3).

These observations suggest that the rMAT ternary complexes contain a low occupancy of the substrates or inhibitors in their active site, and, thus, the binding schemes of ATP, Met, and metals are quite questionable. Interestingly, the rMAT:(ATP+Met+2P_i) complex was formed by soaking ATP into crystals of the rMAT:(Met+2P_i) complex because cocrystallization was not successful, and the active site loop remained disordered, suggesting that the functional state of the enzyme might not have been observed. Therefore, it may not be of functional significance to compare the eMAT ternary complex to the rMAT ternary complexes.

Catalysis Requires Tight Binding of Substrates and the Flexible Loop Movement. On the basis of the structures of eMAT:(ADP+P_i), eMAT:(SAM+PPNP), and eMAT:(AMPPNP+Met) deduced by a modeling study, a detailed catalytic mechanism of SAM formation is proposed here. The enzyme has at least two different conformations primarily due to distinct conformations of the active site loop. One is an open conformation seen in eMAT:(ADP+P_i), in which the flexible loop is disordered, and thus the entrance to the active site is opened. The substrates and products can freely enter or leave the active site. The other one is a closed conformation seen in eMAT:(SAM+PPNP), in which the loop has an ordered conformation and blocks the entrance to the active site (Figure 4). Gln98, Ser99, and Asp101 in the flexible loop are involved in the substrate binding. In the closed conformation, entrance of the substrates into the active site or release the products from the active site are restricted because the active site entrance is blocked.

ATP, 2Mg^{2+} ions, and Met enter the active site when the enzyme has an open conformation. Initially, the tripolyphosphate group of ATP is recognized by basic amino acid residues (His14, Lys165, Arg244, Lys245, Lys265*) and is tightly bound to the protein by hydrogen and ionic bonds. These interactions are consistent with previous mutagenesis studies (*10*). The adenosine moiety of ATP and the Met are then bound to the specific sites, respectively. The adenine ring stacks with the phenyl ring of Phe230, and the 2′-OH and 3′-OH of ribose form hydrogen bonds with Asp163 and Asp238, respectively. The functional significance of these interactions appears to differ since 3′-deoxy-ATP is a good substrate whereas 2′-deoxy-ATP is neither a substrate nor an inhibitor (*5*). The amino and carboxylate groups of Met form hydrogen bonds with acidic amino acid residues (Glu55*, Asp238) and a basic amino acid residue (Lys269*), respectively. In this context, it is noteworthy that the K269M mutated enzyme had a 100-fold increase in the K_M for methionine (*10*). It is noted that Asp238 connects the bound Met and the ribose of ATP through hydrogen bonds. Finally, the flexible loop enters the active site and binds to the substrates through water-mediated hydrogen bonds. The two substrates are now firmly bound to the protein by polar and nonpolar interactions.

Proposed Catalytic Mechanism. As shown in Figure 2, there is no need for significant movement of the adenosine, Met, and PPNP moieties before and after the SAM formation reaction. The major difference is seen in the conformations (C4′-*exo* and C3′-*endo*) of the ribose rings of AMPPNP and SAM. Therefore, it is reasonable to propose the following events: The C5′−O5′ bond of ATP is cleaved simultaneously with formation of the bond between C5′ and the electron-rich S_D of the bound Met by changing the ribose ring conformation from C4′-*exo* to C3′-*endo*.

As shown in Figure 6, the N_{E2} of His14 forms a hydrogen bond with O5′ of AMPPNP (O5′···N_{E2} = 2.85(2) Å), and the N_{D1} of His14 is surrounded by the two amide groups of Asp16 and Lys17 within hydrogen bond distance (N_{D1}···N[Asp16] = 3.05(2) Å, N_{D1}···N[Lys17] = 3.69(2) Å). In this geometry, the imidazole ring of His14 can be

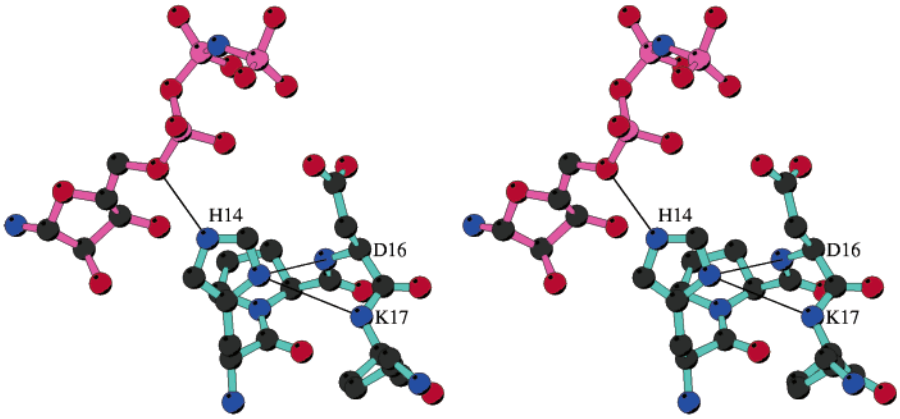

FIGURE 6: A unique geometry of ^{14}His-Pro-Asp-Lys^{17} with the bound SAM and PPNP showing the possible double N−H···N hydrogen bonds which polarize the imidazole ring of His14 to act as an acid in the C5′−O5′ bond cleavage.

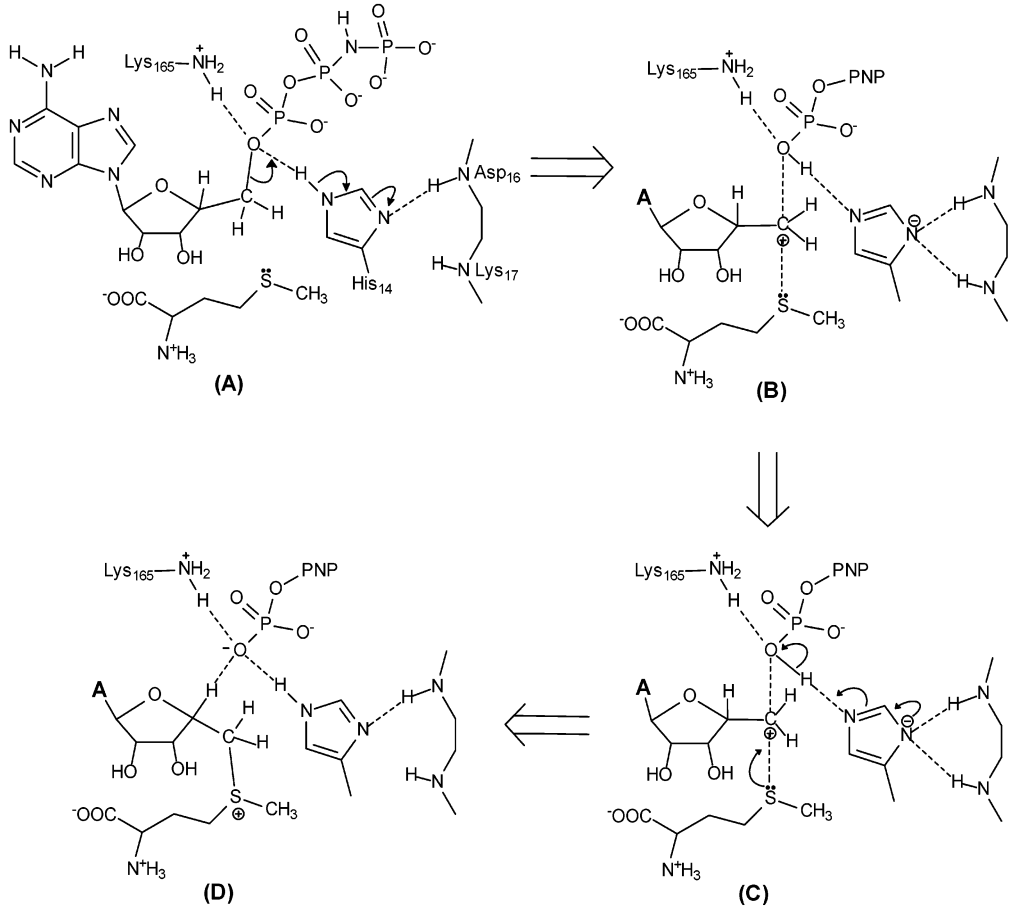

FIGURE 7: Proposed catalytic mechanism for SAM formation. Curved arrows indicate the movements of electron pairs. Possible polar interactions are illustrated by dotted lines. The "+" and "−" indicate positive and negative charges, respectively. Although the mechanism is illustrated in a sequential fashion for clarity, the C5′−O5′ bond cleavage and the C5′−S_D bond formation occur in a concerted manner, i.e., the proposed SAM formation is a S_N2 reaction.

polarized so that the proton on N_{E2} is readily released to O5′ of ATP. The C5′−O5′ bond cleavage is initialized when a molecular vibration allows the amide groups of Asp16 and Lys17 to form strong hydrogen bonds with N_{D1} of His14. Then, a series of electron movements take place from the C_{E1}−N_{D1} bonding electron to the C5′−O5′ bonding electron through the O5′···N_{E2} hydrogen bond, and the C5′−O5′ bond is cleaved and the O5′−H bond is formed in the PPP_i coproduct (Figure 7). The negatively charged N_{D1} of His14 is stabilized by the surrounding basic amide groups of Asp16 and Lys17. The positively polarized C5′ moves toward the electron-rich S_D of the bound Met by changing the ribose ring conformation from C4′-*exo* to C3′-*endo*. The S_D performs a nucleophilic attack on the C5′ to form SAM and displace PPP_i. The negative charge on N_{D1} of His14 moves back to the O5′ of PPP_i and is stabilized by forming a C4′-H···O5′ hydrogen bond (C4′···O5′ = 3.10 Å). Although the mechanism is described above in sequential fashion, the C5′−O5′ bond cleavage and the C5′−S_D bond formation occur in a concerted manner, i.e., the proposed SAM formation is a S_N2 reaction. This proposed catalytic mechanism is consistent with previous mutational studies which

showed >1000-fold reductions in V_{max} when the mutation H14N was made (*10*). In contrast, the V_{max} diminished only 2.5-fold in the K165M mutant, indicating that interactions with Lys165 are of lesser importance in catalysis.

The product SAM in this crystal structure has an S-configuration at the S_D atom, and the naturally occurring SAM has the S-configuration as well (*49*, *50*), supporting the proposed catalytic mechanism. As observed in most nucleoside and nucleotide structures, the glycosidic bonds of ATP and SAM molecules in this crystal structure are anti-conformation. For the overall conformation, the substrate ATP has an extended conformation, whereas the product SAM has a bent conformation. Since SAM and SAH (demethylated SAM) in the known methyltransferase structures (*31*−*48*) and in solution (*14*) have extended conformations, the bent conformation in this structure would be an unfavorable one and would facilitate the release of SAM from the active site. It is noted that SAM can have a bent conformation in the protein complex if it has a rare *syn*-glycosidic bond as seen in the Met repressor complex (*51*).

Proposed Mechanism Is Quite Unique. In general, when a neutral His residue is involved in a general acid−base catalysis, an acidic group polarizes the His residue to act as a base. A typical example is seen in serine protease reaction mechanisms (*52*). In the contrast to the well-known protease examples, we propose that two basic amide groups polarize neutral His14 to act as an acid on the basis of the geometry around the O5′ of AMPPNP/SAM (Figure 6). Lodi and Knowles have proposed a similar catalytic mechanism of triosephosphate isomerase (TIM), in which a neutral His95 acts as an acid (*53*). Interestingly, His95 in the crystal structure of TIM (PDB code: 2YPI) is surrounded by two amide groups of Ser96 and Glu97 with the $N_{D1}\cdots N$ distances of 2.91 and 3.02 Å, respectively (*54*). Since the ^{12}EGHPDK^{17} sequence is conserved in all known MAT genes (*55*−*65*) and TIM has a similar ^{93}LGHSER^{98} sequence, we searched for the sequence GHxYZ (where x = any; Y = acidic residue; Z = basic residue) in the PDB files and found 220 structures. However, none of them except for MAT and TIM has the unique His−amide group interaction.

ACKNOWLEDGMENT

We express our thanks to Professor Richard H. Himes and Richard L. Schowen for a critical reading of this manuscript and very valuable comments.

REFERENCES

1. Cantoni, G. L. (1953) *S*-Adenosylmethionine: A new intermediate formed enzymatically from L-methionine and adenosinetriphosphate. *J. Biol. Chem. 204*, 403−416.
2. Mudd, S. H., and Cantoni, G. L. (1958) Activation of methionine for transmethylation. III. The methionine-activating enzyme of bakers' yeast. *J. Biol. Chem. 231*, 481−492.
3. Parry, R. J., and Minta, A. (1982) Studies of enzyme stereochemistry. Elucidation of the stereochemistry of *S*-adenosylmethionine formation by *Yeast* methionine adenosyltransferase. *J. Am. Chem. Soc. 104*, 871−872.
4. Markham, G. D., Parkin, D. W., Mentch, F., and Schramm, V. L. (1987) A kinetic isotope effect study and transition state analysis of the *S*-adenosylmethionine synthetase reaction. *J. Biol. Chem. 262*, 5609−5615.
5. Markham, G. D., Hafner, E. W., Tabor, C. W., and Tabor, H. (1980) *S*-adenosylmethionine synthetase from *Escherichia coli*. *J. Biol. Chem. 255*, 9082−9092.
6. McQueney, M. S, Anderson, K. S., and Markham, G. D. (2000) Energetics of *S*-adenosylmethionine synthetase catalysis. *Biochemistry 39*, 4443−4454.
7. Markham, G. D. (1981) Spatial proximity of two divalent metal ions at the active site of *S*-adenosylmethionine synthetase. *J. Biol. Chem. 256*, 1903−1909.
8. Zhang, C., Markham, G. D., and Lobrutto, R. (1993) Coordination of vanadyl (IV) cation in complexes of *S*-adenosylmethionine synthetase: Multifrequency electron spin−echo envelope modulation study. *Biochemistry 32*, 9866−9873.
9. Taylor, J. C., Takusagawa, F., and Markham, G. D. (2002) The active site loop of *S*-adenosylmethionine synthetase modulates catalytic efficiency. *Biochemistry 41*, 9358−9369.
10. Taylor, J. C., and Markham, G. D. (2000) The bifunctional active site of *S*-adenosylmethionine synthetase. Roles of the basic residues. *J. Biol. Chem. 275*, 4060−4065
11. McQueney, M. S., and Markham, G. D. (1995) Investigation of monovalent cation activation of *S*-adenosylmethionine synthetase using mutagenesis and uranyl inhibition. *J. Biol Chem. 270*, 18277−18284.
12. Taylor, J. C., and Markham, G. D. (1999) Dissection of the bifunctional active site of *S*-adenosylmethionine synthetase: Roles of the active site aspartates. *J. Biol. Chem. 274*, 32909−32914.
13. Reczkowski, R. S., Taylor, J. C., and Markham, G. D. (1998) The active site arginine of *S*-adenosylmethionine synthetase orients the reaction intermediate. *Biochemistry 37*, 13499−13506.
14. Markham, G. D., Norrby, P.-O., and Bock, C. W. (2002) *S*-adenosylmethionine conformations in solution and in protein complexes: Conformational influences of the sulfonium group. *Biochemistry 41*, 7636−7646.
15. Schalk-Hihi C., and Markham G. D. (1999) The conformations of a substrate and a product bound to the active site of *S*-adenosylmethionine synthetase. *Biochemistry 38*, 2542−2550.
16. Sufrin, J. R., Dunn, D. A., and Marshall, G. R. (1981) Steric mapping of the L-methionine binding site of ATP: L-methionine *S*-adenosyltransferase. *Mol. Pharmcol. 19*, 307−313.
17. Sufrin, J. R., Lombardini, J. B., and Alks, V. (1993) Differential kinetic properties of L-2-amino-4-methylthio-*cis*-but-3-enoic acid, a methionine analogue inhibitor of *S*-adenosylmethionine synthetase. *Biophys. Acta 1202*, 87−91.
18. Ma, Q.-F., Kenyon, G. L., and Markham, G. D. (1990) Specificity of *S*-adenosylmethionine synthetase for ATP analogues mono- and di-substituted in bridging positions of the polyphosphate chain. *Biochemistry 29*, 1412−1416.
19. Kappler, F., Vrudhula, V. M., and Hampton, A. (1988) Toward the synthesis of isozyme-specific enzyme inhibitors. Potent inhibitors of rat methionine adenosyltransferases. Effect of one-atom elongation of the ribose-P^{α} bridge in two covalent adducts of L-methionine and β,γ-imido-ATP. *J. Med. Chem. 31*, 384−389.
20. Kappler, F., Vradhula, V. M., and Hampton, A. (1987) Isozyme-specific enzyme inhibitors. 14. 5′(R)-(C[L-homocysteine-*S*-yl)-methyl]adenosine 5′-(β,γ-imidotriphosphate), a potent inhibitor of rat methionine adenosyltransferases. *J. Med. Chem. 30*, 1599−1603.
21. Takusagawa, F., Kamitori, S., Misaki, S., and Markham, G. D. (1996) Crystal structure of *S*-adenosylmethionine synthetase. *J. Biol. Chem. 271*, 136−147.
22. Takusagawa, F., and Kamitori, S. (1996) A Real knot in protein. *J. Am. Chem. Soc. 118*, 8945−8946.
23. Takusagawa, F., Kamitori, S., and Markham, G. D. (1996) Structure and function of *S*-adenosylmethionine synthetase: Crystal Structure of *S*-adenosylmethionine synthetase with ADP, Br-ADP, PP_i at 2.8 Å resolution. *Biochemistry 35*, 2586−2596.
24. Fu, Z., Markham, G. D., and Takusagawa, F. (1996) Flexible loop in the structure of *S*-adenosylmethionine synthetase crystallized in the tetragonal crystal system. *J. Biomol. Struct. Dyn. 13*, 727−739.
25. González, B., Pajares, M. A., Hermoso, J. A., Alvarez, L., Garrido, F., Sufrin, J. R., and Sanz-Aparicio. J. (2000) The crystal structure of tetrameric methionine adenosyltransferase from rat liver reveals the methionine-binding site. *J. Mol. Biol. 300*, 363−375.
26. González, B., Pajares, M. A., Hermoso, J. A., Guillerm, D., Guillerm, G., and Sanz-Aparicio. J. (2003) Crystal structures of methionine adenosyltransferase complexed with substrates and products reveal the methionine-ATP recognition and give insights into the catalytic mechanism *J. Mol. Biol. 331*, 407−416.

27. Otwinowski, Z., and Minor, W. (1997) Processing of X-ray diffraction data collected in oscillation mode. *Methods Enzymol. 276*, 307−326.
28. Brünger, A. T. (1993) X-PLOR 3.82: A system for X-ray crystallography and NMR, Yale University Press, New Haven and London.
29. Laskowski, R. A., MacArthur, M. W., Moss, D. S., and Thornton, J. M. (1993) ROCHECK: A program to check the stereochemical quality of protein structures. *J. Appl. Crystallogr. 26*, 283−291.
30. Jones, S., and Thornton, J. M. (1995) Protein−protein interactions: a review of protein dimer structures. *Prog. Biophys. Mol. Biol. 63*, 31−65.
31. Zhang, X., Zhou, L., and Cheng, X. (2000) Crystal structure of the conserved core of protein arginine methyltransferase PRMT3. *EMBO J. 19*, 3509−3519.
32. Vidgren, J., Svensson, L. A., and Liljas, A. (1994) Crystal structure of catechol *O*-methyltransferase. *Nature 368*, 354−358.
33. Fu, Z., Hu, Y., Konishi, K., Takata, Y., Ogawa, H., Gomi, T., Fujioka, M., and Takusagawa, F. (1996) Crystal structure of glycine *N*-methyltransferase from rat liver. *Biochemistry 35*, 11985−11993.
34. Schubert, H. L., Wilson, K. S., Raux, E., Woodcock, S. C., and Warren, M. J. (1998) The X-ray structure of a cobalamin biosynthetic enzyme, cobalt-precorrin-4 methyltransferase. *Nat. Struct. Biol. 5*, 585−592.
35. Zubieta, C., He, X. Z., Dixon, R. A., and Noel, J. P. (2001) Structures of two natural product methyltransferases reveal the basis for substrate specificity in plant *O*-methyltransferases. *Nat. Struct. Biol. 8*, 271−279.
36. Klimasauskas, S., Kumar, S., Roberts, R. J., and Cheng, X. (1994) *Hha*I methyltransferase flips its target base out of the DNA helix. *Cell 76*, 357−369.
37. Labahn, J., Granzin, J., Schluckebier, G., Robinson, D. P., Jack, W. E., Schildkraut, I., and Saenger, W. (1994) Three-dimensional structure of the adenine-specific DNA methyltransferase *M. Taq* I in complex with the cofactor *S*-adenosylmethionine. *Proc. Natl. Acad. Sci. U.S.A. 91*, 10957−10961.
38. Reinisch, K. M., Chen, L., Verdine, G. L., and Lipscomb, W. N. (1995) The crystal structure of *Hae*III methyltransferase covalently complexed to DNA: an extrahelical cytosine and rearranged base pairing. *Cell 82*, 143−153.
39. Gong, W., O'Gara, M., Blumenthal, R. M., and Cheng, X. (1997) Structure of *pvu* II DNA-(cytosine N4) methyltransferase, an example of domain permutation and protein fold assignment. *Nucleic Acids Res. 25*, 2702−2715.
40. Tran, P. H., Korszun, Z. R., Cerritelli, S., Springhorn, S. S., and Lacks, S. A. (1998) Crystal structure of the *Dpn*M DNA adenine methyltransferase from the *Dpn*II restriction system of streptococcus pneumoniae bound to *S*-adenosylmethionine. *Structure 6*, 1563−1575.
41. Scavetta, R. D., Thomas, C. B., Walsh, M. A., Szegedi, S., Joachimiak, A., Gumport, R. I., and Churchill, M. E. (2000) Structure of *Rsr*I methyltransferase, a member of the N6-adenine β class of DNA methyltransferases. *Nucleic Acids Res. 28*, 3950−3961.
42. Dong, A., Yoder, J. A., Zhang, X., Zhou, L., Bestor, T. H., and Cheng, X. (2001) Structure of human DNMT2, an enigmatic DNA methyltransferase homolog that displays denaturant-resistant binding to DNA. *Nucleic Acids Res. 29*, 439−448.
43. Hodel, A. E., Gershon, P. D., Shi, X., and Quiocho, F. A. (1996) The 1.85 Å structure of vaccinia protein VP39: a bifunctional enzyme that participates in the modification of both mRNA ends. *Cell 85*, 247−256.
44. Bussiere, D. E., Muchmore, S. W., Dealwis, C. G., Schluckebier, G., Nienaber, V. L., Edalji, R. P., Walter, K. A., Ladror, U. S., Holzman, T. F., and Abad-Zapatero, C. (1998) Crystal structure of ErmC′, an rRNA methyltransferase which mediates antibiotic resistance in bacteria. *Biochemistry 37*, 7103−7112.
45. Bugl, H., Fauman, E. B., Staker, B. L., Zheng, F., Kushner, S. R., Saper, M. A., Bardwell, J. C., and Jakob, U. (2000) RNA methylation under heat shock control. *Mol. Cell 6*, 349−360.
46. Gupta, A., Kumar, P. H., Dineshkumar, T. K., Varshney, U., and Subramanya, H. S. (2001) Crystal structure of Rv2118c: An SAM-dependent methyltransferase from *Mycobacterium tuberculosis* H37Rv. *J. Mol. Biol. 312*, 381−391.
47. Djordjevic, S., and Stock, A. M. (1997) Crystal structure of the chemotaxis receptor methyltransferase CheR suggests a conserved structural motif for binding *S*-adenosylmethionine. *Structure 5*, 545−558.
48. Skinner, M. M., Puvathingal, J. M., Walter, R. L., and Friedman, A. M. (2000) Crystal structure of protein isoaspartyl methyltransferase: A catalyst for protein repair. *Struct. Fold Des. 8*, 1189−1201.
49. Cornforth, J. W., Reichard, S. A., Talalay, P., Carrell, H. L., Glusker, J. P. (1977) Determination of the absolute configuration at the sulfonium center of *S*-adenosylmethionine. Correlation with the absolute configuration of the diastereomeric *S*-carboxymethyl-(*S*)-methionine salts. *J. Am. Chem. Soc. 99*, 7292−7300.
50. Stolowitz, M. L., and Minch, M. J. (1981) *S*-Adenosyl-L-methionine and *S*-adenosyl-L-homocysteine, an NMR study. *J. Am. Chem. Soc. 103*, 6015−6019.
51. Somers, W. S., and Phillips, S. E. (1992) Crystal structure of the Met repressor-operator complex at 2.8 Å resolution reveals DNA recognition by beta-strands. *Nature 359*, 387−393.
52. James, M. N. G., Sielecki, A. R., Brayer, G. D., Delbaere, L. T. J., and Bauer, C. A. (1980) Structure of product and inhibitor complexes of *Streptomyces griseus* protease A at 1.8 Å resolution. *J. Mol. Biol. 144*, 45−88.
53. Lodi, P. J., and Knowles, J. R. (1991) Neutral imidazole is the electrophile in the reaction catalyzed by triosephosphate isomerase: structural origins and catalytic implications. *Biochemistry 30*, 6948−6956.
54. Lolis, E., and Petsko, G. A. (1990) Crystallographic analysis of the complex between triosephosphate isomerase and 2-phosphoglycolate at 2.5 Å resolution: implications for catalysis. *Biochemistry 29*, 6619−6625.
55. Markham, G. D., DeParasis, J., and Gatmaitan, J. (1984) The sequence of *metK*, the structural gene for *S*-adenosylmethionine synthetase in *Escherichia coli*. *J. Biol. Chem. 259*, 14505−14507.
56. Satischandran, C., Taylor, J. C., and Markham, G. D. (1993) Isozymes of *S*-adenosylmethionine synthetase are encoded by tandemly duplicated genes in *Escherichia coli*. *Mol. Microbiol. 9*, 835−846.
57. Peleman, J., Saito, K., Cottyn, B., Engler, G., Seurinck, J., Van Montagu, M., and Inze, D. (1989) Structure and expression analyses of the *S*-adenosylmethionine synthetase gene family in *Arabidopsis thaliana*. *Gene 84*, 359−369.
58. Peleman, J., Boerjan, W., Engler, G., Seurinck, J., Botterman, J., Alliotte, T., Van Montagu, M., and Inze, D. (1989) Strong cellular preference in the expression of a housekeeping gene of *Arabidopsis thaliana* encoding *S*-adenosylmethionine synthetase. *Plant Cell 1*, 81−93.
59. Larsen, P. B., and Woodson, W. R. (1991) Cloning and nucleotide sequence of a *S*-adenosylmethionine synthetase cDNA from carnation. *Plant Physiol. 96*, 997−999.
60. Thomas, D., and Surdin-Kerjan, Y. (1987) SAM1, the structural gene for one of the *S*-adenosylmethionine synthetase in *Saccharomyces Cerevsiae*. *J. Biol. Chem. 262*, 16704−16709.
61. Thomas, D., Rothstein, R., Rosenberg, N., and Surdin-Kerjan, Y. (1988) SAM2 encodes the second methionine *S*-adenosyl transferase in *Saccharomyces Cerevisiae*: physiology and regulation of both enzymes. *Mol. Cell. Biol. 8*, 5132−5139.
62. Horikawa, S., Sasuga, J., Shimizu, K., Ozasa, H., and Tsukada, K. (1990) Molecular cloning and nucleotide sequence of cDNA encoding the rat kidney *S*-adenosylmethionine synthetase. *J. Biol. Chem. 265*, 13683−13686.
63. Horikawa, S., and Tsukada, K. (1993) Molecular cloning and developmental expression of a human kidney *S*-adenosylmethionine synthetase. *FEBS Lett. 312*, 37−41.
64. Horikawa, S., Ishikawa, M., Ozasa, H., and Tsukada, K. (1989) Isolation of cDNA encoding the rat liver *S*-adenosylmethionine synthetase. *Eur. J. Biochem. 184*, 497−501.
65. Horikawa, S., and Tsukada, K. (1991) Molecular cloning and nucleotide sequence of cDNA encoding the human liver *S*-adenosylmethionine synthetase. *Biochem. Int. 25*, 81−90.

BI035611T